doi: 10.18323/2782-4039-2023-1-7-21

The study of the influence of micro-arc oxidation modes on the morphology and parameters of an oxide coating on the D16AT aluminum alloy

Fengyuan Bao[1,3], junior researcher, research engineer
Oleg V. Bashkov*[1,4], Doctor of Sciences (Engineering), Professor,
Head of Chair "Materials Science and Technology of Advanced Materials"
Dan Zhang[2,5], Doctor of Sciences (Engineering), Professor,
Head of "Mechanical Engineering" Laboratory
Lan Lyu[1,2], graduate student
Tatiana I. Bashkova[1,6], PhD (Engineering), Associate Professor
[1]*Komsomolsk-na-Amure State University, Komsomolsk-on-Amur (Russia)*
[2]*Heilongjiang University of Science and Technology, Harbin (China)*

***E-mail: bashkov@knastu.ru**

[3]ORCID: https://orcid.org/0000-0001-5762-7953
[4]ORCID: https://orcid.org/0000-0002-3910-9797
[5]ORCID: https://orcid.org/0000-0003-4150-7038
[6]ORCID: https://orcid.org/0000-0001-7070-5821

Received 06.12.2022 *Accepted 19.01.2023*

Abstract: An effective way to protect valve metals and their alloys is the micro-arc oxidation method (MAO), which is currently used in various industries. However, to achieve the desired characteristics and properties of oxide coatings, a large number of experiments are required to determine an optimal oxidation mode, which makes the MAO method labor-intensive and resource-consuming. One of the ways to solve this problem is the search for an informative parameter or several parameters, the use of which during the oxidation process monitoring allows identifying a relationship between the MAO modes and the specified characteristics of oxide coatings. This paper studies the influence of the specified technological MAO modes (current density, oxidation time, amplitude of acoustic emission (AE) signals recorded during MAO) on the morphology and parameters of oxide coatings (thickness δ and surface roughness R_a) deposited on the D16AT aluminum alloy clad with pure aluminum. Multivariate planning of an experiment and the performed regression analysis allowed establishing a relationship between two oxidation factors (current density and oxidation time) and the parameters of the produced coatings. The authors proposed an additional factor, which is determined in the monitoring mode during the oxidation process as the time from the moment when the maximum or minimum of the acoustic emission (AE) amplitude recorded in the MAO process is reached until the end of the oxidation process. The study established that the introduction of an additional factor allows increasing significantly the reliability of the dependence between the coating parameters obtained experimentally and by the computational method based on the regression analysis. The authors note that when performing MAO, with the additional use of the MAO process monitoring by recording the AE amplitude, it is possible to achieve a high reliability between the calculated and actual values of the parameters of oxide coatings.

Keywords: micro-arc oxidation; oxide coating; acoustic emission; multivariate analysis; surface morphology; aluminum alloy; D16AT alloy; valve group alloy.

Acknowledgements: The work was supported by the Presidential grant for government support of leading scientific schools of the Russian Federation (project NSh-452.2022.4).

For citation: Bao F., Bashkov O.V., Zhang D., Lyu L., Bashkova T.I. The study of the influence of micro-arc oxidation modes on the morphology and parameters of an oxide coating on the D16AT aluminum alloy. *Frontier Materials & Technologies*, 2023, no. 1, pp. 7–21. DOI: 10.18323/2782-4039-2023-1-7-21.

INTRODUCTION

Coatings produced by micro-arc oxidation (MAO) on the parts made of metals and alloys of the valve group, distinguishing by many valuable working and service properties (wear resistance, heat resistance, electrical insulating properties), have a special place among the surface treatment methods used in industry. The MAO method, similar to anodic oxidation, involves the oxidation of the surfaces of such metals as aluminum, magnesium, titanium, and other valve metals under the action of the electric current in an electrolyte. Compared to anodic oxidation, during MAO, the mixtures of various types of salts or alkalis with a low concentration are used and not the concentrated acids. Oxidation is carried out under the action of micro-arc discharges formed by a high voltage pulse generator of positive polarity. The pulse amplitude can reach 400–600 V [1], and the pulse repetition rate depends on a generator type. At present, the MAO technology is not widely used for some reasons, including the lack of systematization of the relationship between parameters, which would contain practical recommendations for achieving the optimal oxidation regime [2].

Initially, it was believed that the MAO technology optimization should be based only on an in-depth study of the MAO mechanism to identify the oxide coating

formation process. The research in this area has indeed achieved significant results at the early stage of the MAO technology development. For example, the effective components in the electrolyte participating in the MAO process are determined based on the study of the electrochemical reaction principle. The direction of optimizing the power supply for MAO is determined based on the study of the electrical breakdown mechanism [3–5].

However, when studying the micro-arc oxidation mechanism, various models of interpretation of the oxide coating formation process appeared. The models accepted by the majority of scientists include the model of bubble breakdown on the anode, the model of oxide formation on the anode using the breakdown voltage U_B, the models based on the tunnel and avalanche effects, etc.

The development of basic research on the MAO technology is rather limited by the lack of a unified theoretical model. In recent years, the volume of study of the MAO mechanism has been gradually decreasing. At the same time, a large number of studies are focused on the optimal selection of the MAO process parameters using the optimization method. In most existing works, the method of planning of a multifactorial experiment is used, followed by determining the correlation between the processing factors and the parameters of the resulting coating properties. This allows establishing technical criteria for the efficient production management under certain conditions [6–8]. Such studies contributed to a significant development of MAO technology and allowed applying MAO in various industries.

However, due to the variety of MAO factors influencing the properties and parameters of the formed oxide coatings, and types of the widely used alloys of valve metals, it is necessary to carry out systematic studies, including the experiments under various conditions and using the effective methods for analyzing the results [9].

Today, the search for an associate parameter combined with the processing factors, which would ensure the complex of properties of the coatings produced with the MAO technology in real time, has become a promising direction of the study aimed at solving the noted problems. Based on this concept, various methods for controlling the MAO process were proposed: the method of monitoring the electrical parameters in the reverse circuit [10], the method of visual control of micro-arcs using a high-speed photo camera [11], the method of inductive measurement of the coating thickness in real time [12], and the method of accumulation of acoustic emission events during MAO [13–15].

According to the breakdown theory, the growth of oxide coatings is based on the formation of oxides melted after a high-voltage breakdown and solidified on the oxide metal surface. The energy dissipated during a discrete high-voltage breakdown is mainly converted into temperature, and some of the energy is converted into elastic waves propagating in the material. Acoustic emission (AE) signals recorded in the MAO process can carry the information about the source of a discrete electrical breakdown in the MAO process [16]. Therefore, the parameters of the recorded AE signals can be used to describe the kinetics of the oxide coating growth in real time.

Special features of the MAO technology make it difficult to control any parameters of a formed coating during processing. The surface thickness and roughness are one of the most requested parameters determining the properties and quality of the MAO-produced oxide coatings. These parameters are most often found in the literature and characterize MAO coatings to the fullest extent from the technological and operational point of view.

The study is aimed to establish the dependence of the oxide coating thickness and roughness on the micro-arc oxidation modes and to search for the possibility of controlling the parameters of a formed oxide coating in real time using the acoustic emission method.

METHODS

Materials and samples

Plates 2 mm thick, 20×20 mm in size cut from a D16AT aluminum alloy sheet in a naturally aged state and clad on both sides with pure aluminum 100 μm thick were used as the samples for the oxidation.

Micro-arc oxidation unit

The MAO implementation scheme is shown in Fig. 1. Using a clamp, the sample is fixed in the electrolyte bath. An acoustic emission transducer (AET) is connected to a broadband amplifier and mounted on the sample above the clamp to prevent electrolyte from getting on the AET body, which is electrically isolated from the sample. The module for registration and control of the MAO system carries out the control of the MAO unit power source, the registration of the oxidation electrical parameters (voltage, current), as well as the registration of AE signals during the oxidation process. The MAO system can be used in two modes: voltage constraints and maximum current constraints. It gives the possibility to control the nature and mechanism of the oxide film growth.

The device ensures the formation of single-polarity pulses of positive polarity. The unit scheme is based on a three-phase double-wave rectifier with thyristor control. The electronic circuit diagram of the unit operates under the control of a computer with specially configured software. The rectifier generates voltage pulses with a frequency of 300 Hz and adjustable duration, which is determined by the oxidation current or voltage in accordance with the specified mode. In the work, the maximum current constraint mode was used.

To prevent the electrolyte from heating above 40 °C during oxidation, its thermostat control with the help of a water-cooling coil located in a stainless steel bath and acting as a cathode was used. For all the samples, MAO was performed in an electrolyte of the composition Na_2SiO_3 + KOH + distilled water [17; 18].

Registration and analysis of AE signals were performed using a system based on the Adlink PCI-9812 analog-to-digital converter and AE Pro 2.0 software. The GT301 broadband AET with a frequency range of 50–550 kHz was used as an AE transducer. The amplification factor of the AE signal amplifier was 40 dB. The AET was mounted on a D16AT aluminum alloy plate, which was a continuation of the sample.

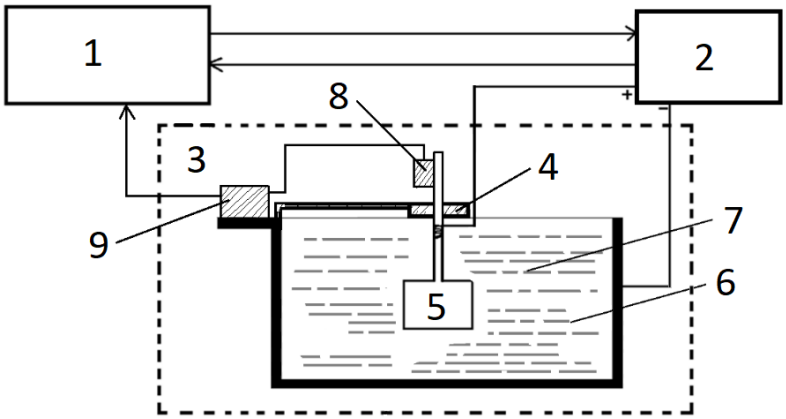

Fig. 1. *The scheme of a unit for MAO and data registration:*
1 – registration and control module; 2 – power source; 3 – oxidation cell;
4 – clamp; 5 – sample; 6 – bath; 7 – electrolyte;
8 – acoustic emission transducer (AET); 9 – amplifier
Рис. 1. *Схема установки МДО и регистрации данных:*
1 – модуль регистрации и управления; 2 – источник питания; 3 – ячейка для выполнения оксидирования;
4 – фиксатор; 5 – образец; 6 – ванна; 7 – электролит;
8 – преобразователь акустической эмиссии (ПАЭ); 9 – усилитель

The experiment method

In this work, the application of the technique of multi-factorial planning and analysis allowed determining the degree of interrelation between the MAO process factors, as well as their influence on the parameters of the produced oxide coatings. The oxidation current density value *i* and the oxidation time *t* were the variable factors.

The oxidation modes specified by the two-factor experiment planning matrix are shown in Table 1.

During oxidation, the actual value of the oxidation pulse voltage U_D was recorded at the load in the return circuit. This parameter is necessary to control the MAO process after establishing the relationships between the specified modes and the target values of the coating parameters.

After oxidation carried out in the planned modes, the samples were washed in the distilled water and degreased. After that, the surface was analyzed using the Hitachi S-3400N scanning electron microscope (SEM) in two modes: the secondary electron (SE) mode to observe channels formed as a result of MAO, and the back-scattered electron (BSE) mode to study the surface topography. Thickness δ and surface roughness R_a were chosen as informative parameters of the resulting oxide coating. The thickness of the coatings was determined by SEM after the preparation of transverse sections. Roughness R_a was determined with the TR200 portable roughness meter.

To establish the relationship between the specified MAO modes and the parameters of the produced oxide

Table 1. *The experiment factor planning matrix*
Таблица 1. *Матрица факторного планирования эксперимента*

Factor	**Samples**								
	*D*1	*D*20	*D*10	*D*11	*D*5	*D*19	*D*12	*D*21	*D*9
Current density *i*, A/dm^2	22			48			74		
Treatment time *t*, s	180	900	1620	180	900	1620	180	900	1620

Note. A number after the letter D in the designation of samples indicates the numerical order of a test series conducted during the research and is not associated with the number of experiment factor planning. At least three experiments were performed in each series to ensure its statistical repeatability and reliability.

Примечание. Цифра после буквы D в обозначении образцов означает порядковый номер серии испытаний, проводимых во время исследований, и не связана с номером факторного планирования эксперимента. В каждой серии выполнялось как минимум по три эксперимента, позволяющих обеспечить его статистическую повторяемость и достоверность.

coatings, the regression analysis was used. The technique consists in solving the linear regression equations using the parameters of the MAO modes (oxidation current density i and oxidation time t) as the input variable factors, as well as the values of the parameters of the produced oxide coatings (thickness δ, surface roughness R_a) as the output results. The novelty of the study is in the use of an additional factor – the AE amplitude recorded in the monitoring mode during the entire oxidation process.

In addition to the parameters of the current density and the total oxidation time, a parameter was used that was defined as a period of time from the moment of cyclic change in the AE amplitude recorded in the MAO process to the end of the oxidation process. The paper considers the results of the study of oxide coatings produced depending on the specified MAO modes. Various periods of a cyclic change in the AE amplitude were used as an additional factor. The proposed approach allows increasing the reliability between the calculated and experimental values of the oxide coating parameters.

RESULTS

According to the modes specified in Table 1, the experiments on the deposition of MAO coatings were carried out. Depending on the specified modes, the effective value of the pulse oxidation voltage U_D, that is an important parameter determining the nature of the oxide coating formation due to the spark and micro-arc discharges on the surface of a passivated metal, changed during the oxidation process. A time dependence $U_D(t)$ typical view for a sample oxidized at the current density i=48 A/dm^2 is shown in Fig. 2. The arrows in figure indicate the oxidation time periods for the samples: t=180 s is for D11, t=900 s is for D5, and t=1620 s is for D19.

Fig. 3 shows the SEM images of the surface of MAO coatings produced in accordance with the modes indicated in Table 1, at the current density i=48 A/dm^2 and time limits indicated in Fig. 2.

Fig. 3 shows that the surface uniformity decreases significantly with an increase in the processing time. In the MAO initial period, the low breakdown voltage does not lead to the formation of molten oxides on the sample surface due to the low intensity of micro-arc discharges. Moreover, practically the same dielectric properties of an oxide layer along the entire surface make it possible to uniformly distribute a dense grid of micro-arc discharges over the sample. However, the increased current density in the substrate protruding parts leads to a relatively rough surface in local areas. In general, the roughness of the initial substrate surface influences greatly the quality of a resulting MAO coating, since the oxide coating morphology at this stage repeats the substrate surface, enhancing the relief.

Fig. 3 c shows the coating surface morphology at the next oxidation stage limited by the experiment time constraints (sample D19 in Fig. 2). According to the image obtained using SEM in the SE mode, the diameter of channels in this oxidation period practically did not increase. However, the relief unevenness and the distribution of channels over the surface caused by the formation of molten oxides overlapping the existing channels resulting from local intense micro-arc discharges increased. The uneven distribution of breakdown sites led to a significant increase in the coating surface roughness.

Three-dimensional graphs obtained using the cubic interpolation of experimental data and shown in Fig. 4 allow visualizing the dependence of values of the oxide coating parameters (δ and R_a) obtained after oxidation on the MAO modes (i, t). This is necessary when choosing the range of optimal processing parameters. In the 3-D dependence graphs, the dots mark the experimental values of the measured parameters obtained under the specified MAO modes.

The 3-D dependences show that the δ and R_a values do not have the same growth function of the measured parameter on the given factors (i, t) within the entire range [19], and in a certain range of the factors' values, a significant change in the δ and R_a parameters is not observed.

To establish the relationship between the MAO modes and the parameters of the produced coatings, a regression analysis was carried out. The resulting regression equations of the coating δ and R_a parameters measured during MAO and one of the oxidation electrical parameters (the effective value of the pulse oxidation voltage U_D) are presented in the formulas:

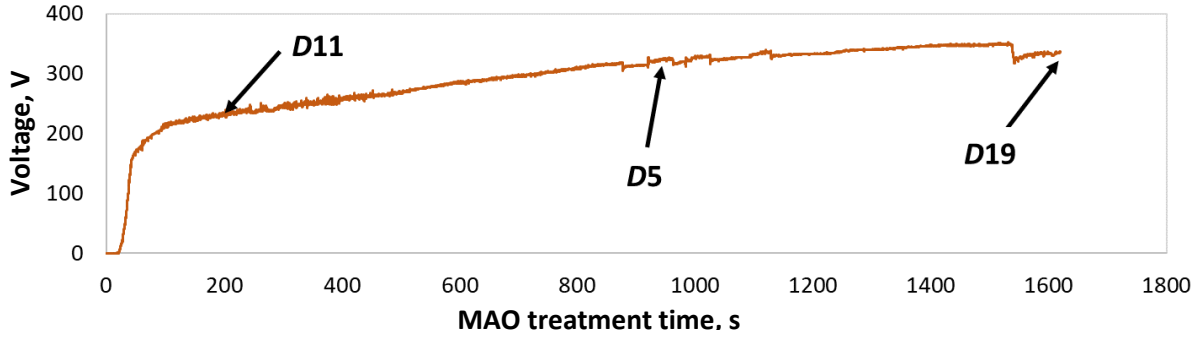

Fig. 2. *The diagram of the voltage dependence on the MAO time*
Рис. 2. *Диаграмма зависимости напряжения от времени МДО*

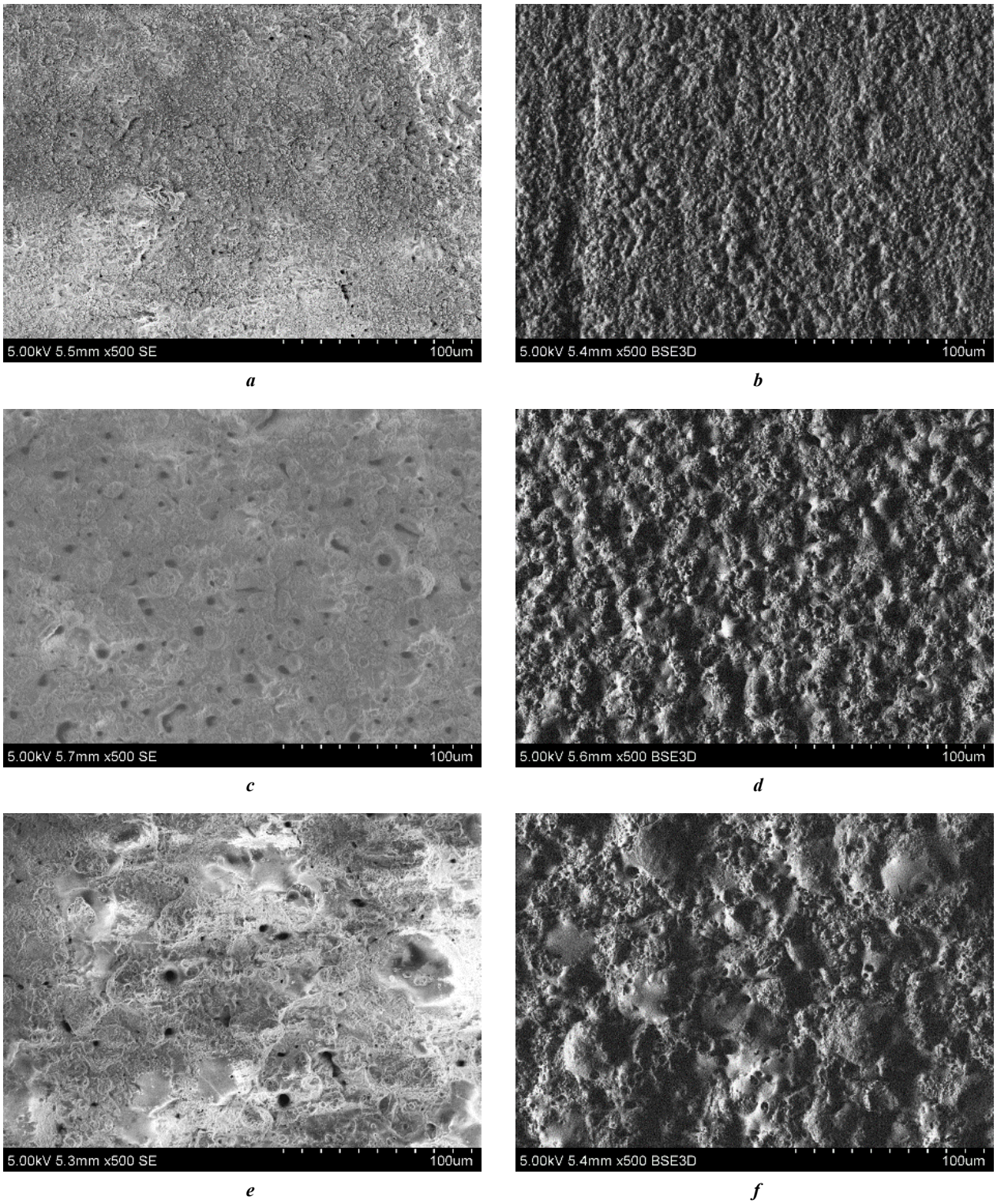

a ***b***

c ***d***

e ***f***

Fig. 3. *MAO-coating surface morphology for the samples:*
a, ***b*** *– D11;* ***c***, ***d*** *– D5;* ***e***, ***f*** *– D19*
Рис. 3. *Морфология поверхности МДО-покрытия для образцов:*
a, ***b*** *– D11;* ***c***, ***d*** *– D5;* ***e***, ***f*** *– D19*

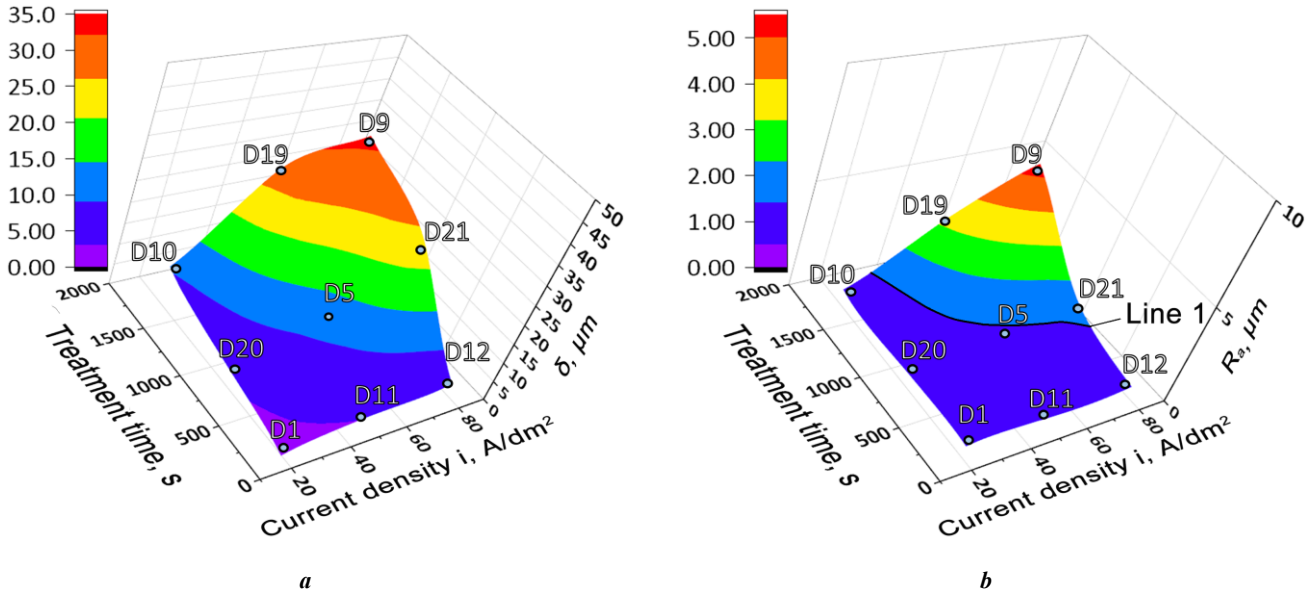

a *b*

Fig. 4. *3-D dependences of the MAO-coating parameters on the specified factors:* ***a*** *–* $\delta(i, t)$*;* ***b*** *–* $R_a(i, t)$

Рис. 4. *Трехмерные зависимости параметров МДО-покрытий от заданных факторов:* ***а*** *–* $\delta(i, t)$*;* ***b*** *–* $R_a(i, t)$

$$\delta = -12{,}199 + 0{,}2819 \times i + 0{,}0123 \times t;$$

$$R_a = -1{,}275 + 0{,}0327 \times i + 0{,}0015 \times t;$$

$$U_D = 95{,}37 + 2{,}1875 \times i + 0{,}0757 \times t.$$

Table 2 shows the coating δ and R_a parameters obtained experimentally and calculated by solving the linear regression equations using the corresponding MAO modes for each sample.

Fig. 5 a shows that the dependences of both the experimental and calculated values of the coating thickness δ on the stress U_D have a rather high reliability of linear approximation and practically converge with each other. The dependences of the experimental and calculated values of the R_a roughness on the U_D voltage do not coincide according to the linear approximation graphs (Fig. 5 b), which is explained by the heredity of the sample surface relief at a low thickness of the oxide coating.

However, from a practical perspective, the relationship between the "experimental" and "calculated" values of the oxide coating parameters (Fig. 6) can be an informative graph used for the assessment of the reliability of using a linear regression model.

The displayed dependences show that the use of a linear regression model to determine δ and R_a, by calculation and experimentally, had poor accuracy (error level – 0.9 and 0.8, respectively). In this regard, the authors decided to use additional parameters obtained using the AE method.

Fig. 7 shows the time diagrams for the amplitude of the AE signals recorded during the MAO process. The signals are single pulses following periodically during the entire period of oxidation. The AE signal repetition period depends on the frequency of the pulse generator of the MAO unit. The amplitude and other AE signal parameters depend on the mode and features of oxidation. As for the time dependence of the AE signal amplitude (Fig. 7), the diagrams show the differences depending on the specified values of the current i and the time t passed from the oxidation onset. It should be noted that the nature of the change in the amplitude of the AE signals recorded in the initial oxidation period retains regardless of the current density i. Depending on the oxidation modes, several cycles of the increase and subsequent decrease in the amplitude of the recorded AE signals can be observed. However, the period when the cycle of change in the AE amplitude proceeds is different for different values of the oxidation current density.

The process of changing the amplitude of the recorded AE signals can be divided into 4 stages. The boundaries of the stages are marked with letters and compared to the change in time of the recorded voltage U_D value. For the quantitative assessment of the values of the AE amplitude recorded during the MAO process, the authors used as an additional new factor the values of the time periods (*AN*, *BN*, and *CN*) from the end of each of the stages (*OA*, *AB*, and *BC*, respectively) to the end of the MAO process. These periods were used to construct the linear regression equations and are shown in Table 3 as the oxidation factors P_1, P_2, and P_3.

It should be noted that in Table 3, the values of the P_2 and P_3 parameters are actually absent for some modes. This is caused by the fact that when selecting the modes with a short oxidation time or low current density, the oxidation process may not reach the P_2 or P_3 stage.

The linear regression equations when calculating the values of the coating parameters using the P_1 factor take the form:

$$\delta = 11{,}922 + 0{,}018 \times i - 0{,}2267 \times t + 0{,}2426 \times P_1;$$

$$R_a = 2{,}3277 - 0{,}0067 \times i - 0{,}0344 \times t + 0{,}0362 \times P_1.$$

Table 2. *Values of MAO-coating parameters*
Таблица 2. *Значения параметров МДО-покрытия*

Sample No.	MAO-coating parameters					
	Experimental values			Calculated values		
	δ, μm	R_a, μm	$U_Д$, V	δ, μm	R_a, μm	$U_Д$, V
***D*20**	5.4±0.8	0.77±0.08	198±10	6.33	0.79	212
***D*10**	10.1±2.1	0.87±0.10	254±14	16.20	1.87	266
***D*11**	4.1±1.0	0.71±0.11	254±14	3.80	0.56	214
***D*5**	12.4±2.2	1.33±0.22	281±14	13.67	1.64	269
***D*19**	28.4±2.7	3.16±0.34	348±15	23.53	2.72	323
***D*12**	5.5±1.0	0.83±0.11	254±12	11.41	1.45	273
***D*21**	24.6±2.6	1.84±0.25	343±16	21.27	2.53	328
***D*9**	32.1±2.7	4.97±0.36	362±16	31.14	3.61	382

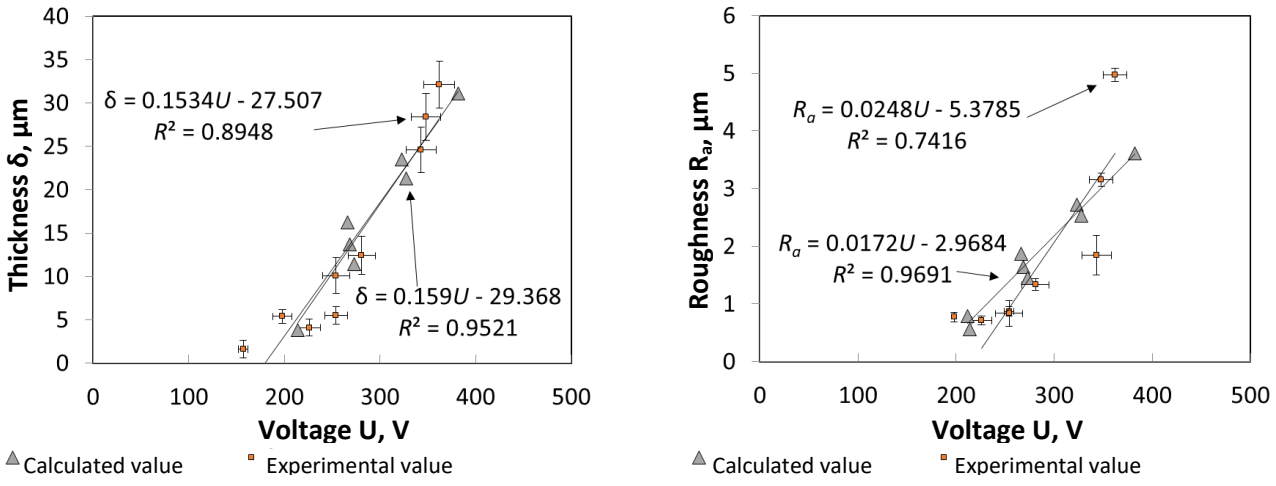

a ***b***

Fig. 5. *The dependences of experimental and calculated values of the parameters of coatings on the voltage U_D:*
a *– $\delta(U_D)$;* ***b*** *– $R_a(U_D)$*
Рис. 5. *Зависимости экспериментальных и расчетных значений параметров покрытий от напряжения U_D:*
a *– $\delta(U_D)$;* ***b*** *– $R_a(U_D)$*

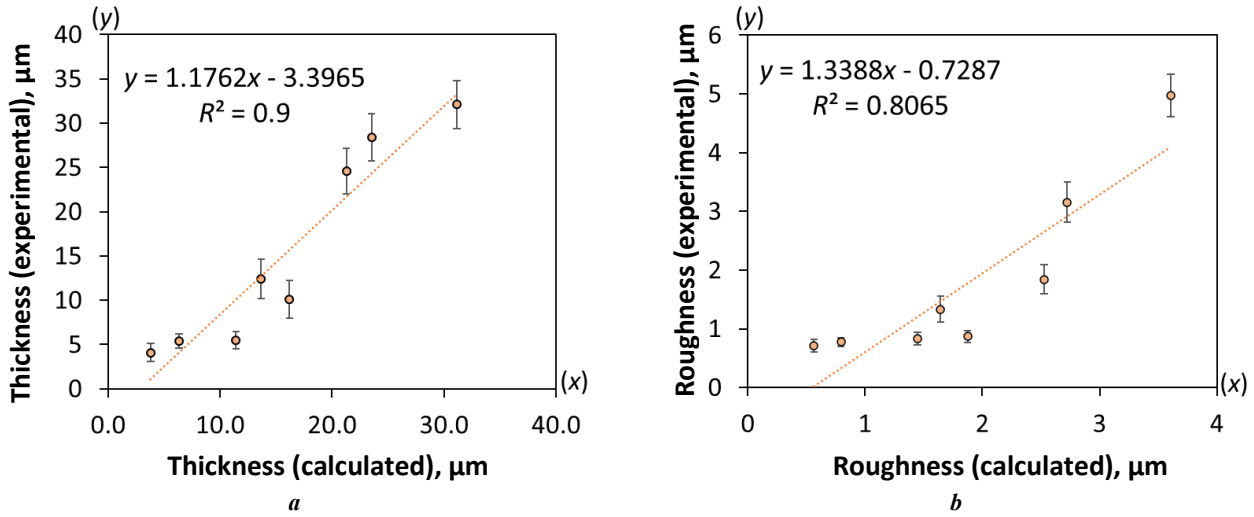

Fig. 6. *A graph relating the experimental and calculated values of the MAO-coating parameters:*
a *– coating thickness;* ***b*** *– coating roughness*
Рис. 6. *График, связывающий экспериментальные и расчетные значения параметров МДО-покрытия:*
a *– толщина покрытия;* ***b*** *– шероховатость покрытия*

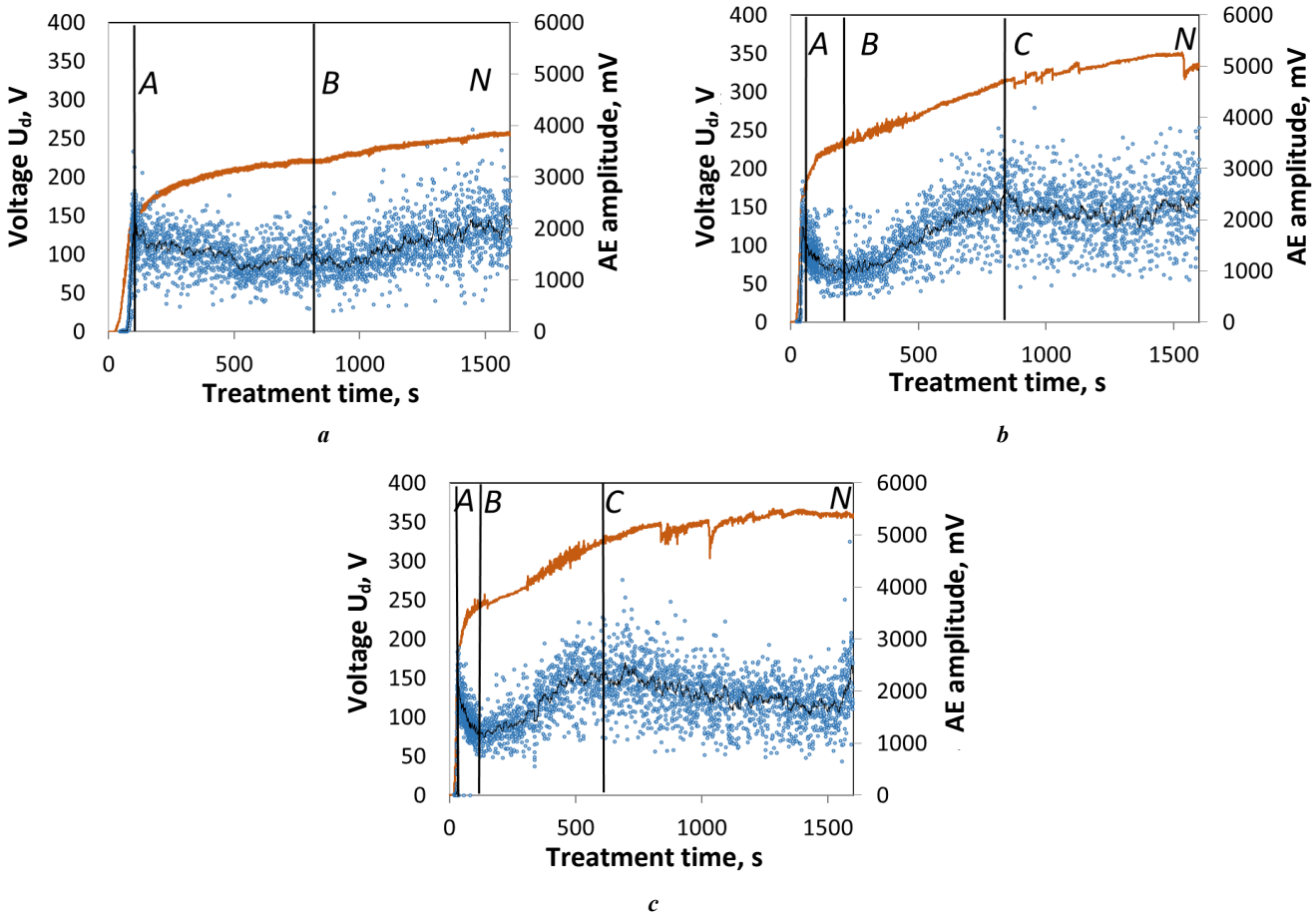

Fig. 7. *Time diagrams of the AE amplitude and oxidation voltage registered during MAO:*
a *– sample D10;* ***b*** *– sample D19;* ***c*** *– sample D9.*
In the diagrams: A – the boundary of the 1 and 2 stages; B – the boundary of the 2 and 3 stages;
C – the boundary of the 3 and 4 stages; N – MAO process termination
Рис. 7. *Диаграммы временных зависимостей амплитуды АЭ и напряжения оксидирования, регистрируемых в процессе МДО:*
a *– образец D10;* ***b*** *– образец D19;* ***c*** *– образец D9.*
На диаграммах: A – граница стадий 1 и 2; B – граница стадий 2 и 3;
C – граница стадий 3 и 4; N – завершение процесса МДО

Table 3. *AE parameters*
Таблица 3. *Параметры АЭ*

Oxidation period, s	Sample No.								
	***D*1**	***D*20**	***D*10**	***D*11**	***D*5**	***D*19**	***D*12**	***D*21**	***D*9**
AN (P_1)	109±5	808±7	1515±8	135±7	859±6	1575±5	151±7	868±8	1587±5
BN (P_2)	–	400±15	690±20	–	700±18	1394±16	46±10	768±14	1479±14
CN (P_3)	–	–	–	–	70±23	795±20	–	258±18	984±21

The linear regression equations when calculating the values of the coating parameters using the P_2 factor take the form:

$$\delta = -7{,}8397 + 0{,}018 \times i - 0{,}0014 \times t + 0{,}0174 \times P_2;$$

$$R_a = -1{,}2374 - 0{,}0229 \times i + 0{,}00000955 \times t + 0{,}0026 \times P_2.$$

The linear regression equations when calculating the values of the coating parameters using the P_3 factor take the form:

$$\delta = -0{,}0001 + 60{,}3825 \times i + 8{,}5813 \times t - 8{,}5 \times P_3;$$

$$R_a = 1528{,}2181 - 9{,}1459 \times i - 1{,}31 \times t + 1{,}3 \times P_3.$$

Table 4 gives the values of the coating δ and R_a parameters obtained experimentally and calculated by solving the above equations using an additional factor.

At the first stage *OA* up to a voltage of 150–250 V, at a certain point, a rather rapid growth of the signal amplitude to the values of 2500–3000 mV begins. Then, the signal amplitude starts to gradually decrease. The greater is the oxidation current density, the higher is the decrease rate. Hereinafter, the amplitudes of the signals recorded by the GT301 model AET mounted on a duralumin plate, acting as a waveguide and being a continuation of the sample used in the oxidation, are given. After a certain oxidation time, the amplitude of the recorded signals reaches a certain minimum (*AB* stage), following which, the amplitude growth resumes and reaches a new maximum (*BC* stage). Further, depending on the MAO duration, the process of changing the amplitude of the recorded AE signals can reoccur. One more full cycle of the decrease and subsequent increase in the amplitude is observed during the oxidation of samples with a current density of 48 and 74 A/dm^2.

Fig. 7 demonstrates that at the initial stage *OA*, at a high rate of the oxidation voltage U_D growth, the formation of a barrier film and the appearance of a luminescence begin on the anode surface, accompanied by the formation of a large number of small bubbles. The amplitude of the recorded AE signals starts from 5–50 mV at the beginning and rapidly increases to 2300 mV by the end of the *OA* stage.

Fig. 8 shows the graphs relating the experimental and calculated values of the MAO-coating parameters with the participation of the AE P_1 factor as an additional factor in the regression calculation. The *OA* stage boundary for determining the P_1 parameter is the achievement of the maximum AE amplitude values in the first cycle of the AE amplitude change during the oxidation period.

Using the P_1 stage achievement time, it can be identified that the reliability of the linear approximation between the calculated and experimental values of the thickness δ and oxide coating roughness R_a is much higher (Fig. 8) compared to the results of the regression calculation without the additional P_1 factor (Fig. 6).

The three-dimensional dependence in Fig. 4 illustrates that the coating roughness increases sharply when a certain critical line 1 is reached under the action of two factors. However, during the oxidation period corresponding to the first stage *OA* (Fig. 7 a), no sharp increase in the coating roughness R_a is observed, since during this period, a barrier layer is formed without the stable growth of the oxide coating, and the roughness is determined by the hereditary relief of the sample surface prepared before oxidation.

Therefore, the results of linear regression by the P_1 factor characterizing the coating roughness have a rather low value of the reliability of the linear approximation R^2=0.8217 with the experimental values (Fig. 8 b).

At the *AB* stage (Fig. 7 c), when the breakdown potential of the passivating film is reached, spark discharges gradually appear on the anode surface. The average value of the AE amplitude at the *AB* stage decreases to a value of 800 mV, which is minimal in the first cycle of changing the AE signals amplitude.

Fig. 9 shows the graphs relating the experimental and calculated values of the thickness δ and roughness R_a of the coating when using the AE P_2 factor in the regression analysis. As opposed to the P_1 factor, the time period determined by the change in the amplitude of the recorded AE signals shifts to the right along the time axis and is defined as the *BN* period from the moment the *AB* stage is completed to the end of MAO. The *AB* stage boundary for determining the P_2 parameter is the achievement of the minimum AE amplitude values at the beginning of the second cycle of the AE amplitude change.

It should be noted that the P_1 factor determined by the initial stage of treatment includes both the MAO period and the period when a sample reaches the passivation

Table 4. *Test results*
Таблица 4. *Результаты эксперимента*

Sample No.	Experimental values		Calculated values					
	δ, μm	R_a, μm	δ, μm			R_a, μm		
			P_1	P_2	P_3	P_1	P_2	P_3
***D*20**	5.4±0.8	0.77±0.08	4.3	4.4	–	0.5	0.31	–
***D*10**	10.1±2.4	0.87±0.10	12.6	10.4	–	1.3	1.07	–
***D*11**	4.1±1.0	0.71±0.11	4.7	–	–	0.7	–	–
***D*5**	12.4±2.5	1.33±0.22	17.2	14.5	16.7	2.1	1.70	1.32
***D*19**	28.4±2.7	3.16±0.34	27.6	27.5	32.7	3.3	3.51	3.14
***D*12**	5.5±1.0	0.83±0.11	9.1	7.0	–	1.1	0.60	–
***D*21**	24.6±2.8	1.84±0.25	19.8	20.5	28.9	2.3	2.49	1.83
***D*9**	32.1±2.7	4.97±0.36	31.0	33.9	36.4	3.5	4.35	4.95

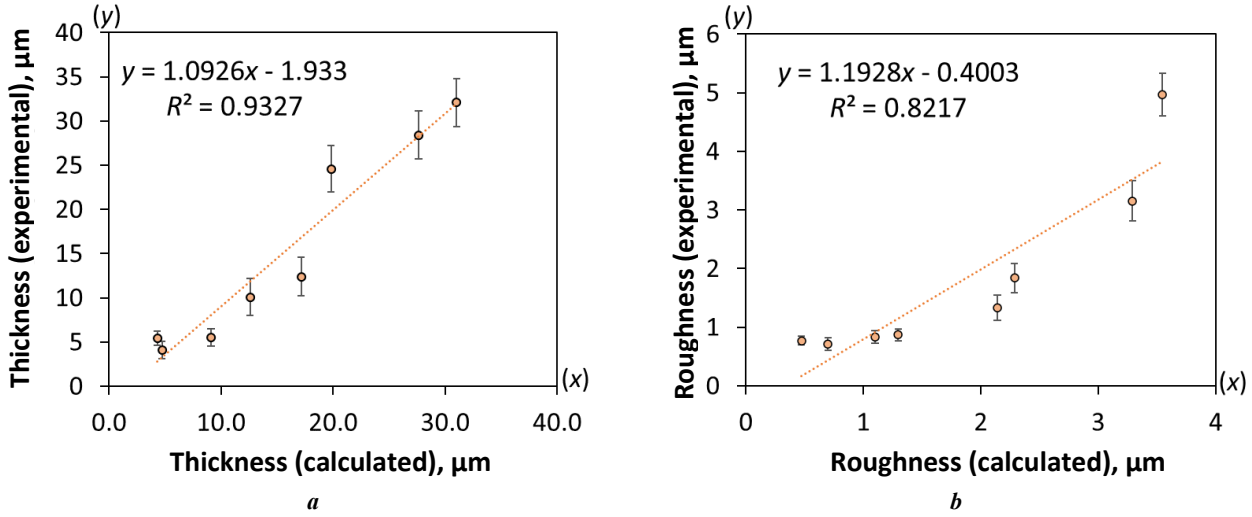

Fig. 8. *A graph relating the experimental and calculated values of the thickness δ (**a**) and roughness R_a (**b**) of the coating with the participation of the P_1 factor*
Рис. 8. *График, связывающий экспериментальные и расчетные значения толщины δ (**a**) и шероховатости R_a (**b**) покрытия при участии фактора P_1*

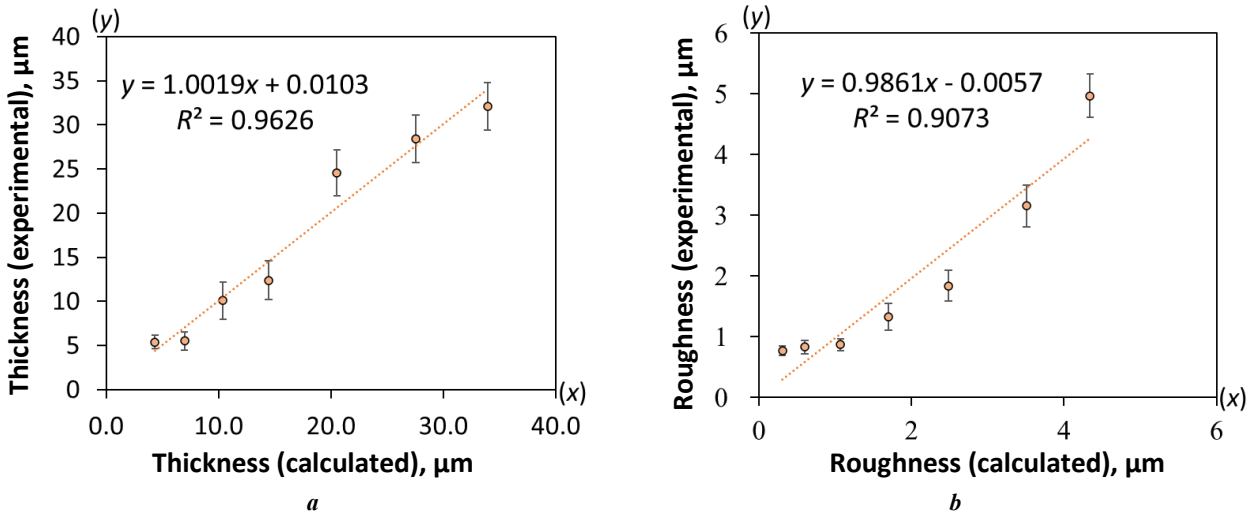

Fig. 9. *A graph relating the experimental and calculated values of the thickness δ (**a**) and roughness R_a (**b**) of the coating with the participation of the P_2 factor*
Рис. 9. *График, связывающий экспериментальные и расчетные значения толщины δ (**а**) и шероховатости R_a (**b**) покрытия при участии фактора P_2*

potential, during which there is no stable growth of the oxide coating due to the MAO mechanism. Therefore, the use of the P_2 parameter as compared to P_1, which is determined by the processing time during the *BN* period, makes it possible to further increase the reliability of the approximation between the values of the calculated and experimental data for determining the coating thickness and roughness.

At the *BC* stage (Fig. 7), the average amplitude of the AE signals increases as the oxidation voltage increases up to a maximum value of 2500 mV with a large dispersion of values. An increase in the signal amplitude occurs with a simultaneous increase in the size and brightness of individual micro-arc discharges on the anode surface.

Fig. 10 presents a graph relating the experimental and calculated values of the coating thickness δ and roughness R_a when using the additional P_3 factor in the regression analysis. The achievement of the maximum AE amplitude values in the second cycle of the AE amplitude change during MAO is the boundary of the *BC* stage for determining the P_3 parameter. The *CN* period is defined from the end of the *BC* stage to the end of MAO.

Fig. 7 b, 7 c show that the *C* boundary shifts backward along the time axis with an increase in the current density *i*. In combination with the analysis presented in Fig. 4 b, 4 c, one can see that for different samples, the time points determined by the *C* stage boundary almost coincide in the same range of two contour lines of the δ value change. It indicates that there is a relationship between the *CN* period, determined according to the AE amplitude change, and the coating thickness δ.

The abovementioned analysis proves that the P_3 factor has a closer relationship with the MAO-coating parameters than the P_1 and P_2 factors. Using the P_3 stage achievement time as an additional factor in solving the linear regression equations, as shown in Fig. 9, it is possible to achieve the approximation reliability equal to 1 between the values of the calculated and experimental data on the coating thickness and roughness.

DISCUSSION

The results of the analysis of three-dimensional dependences showed that the change in the coating thickness and roughness is nonlinear within the range of the oxidation period t=180–1620 s and the current density i=22–74 A/dm^2. This makes it inappropriate to use a linearly changing parameter (processing time, current density) to establish the dependences of the resulting coating parameters on the MAO modes.

One of the conventional solutions to this problem is the use of a non-linear variable concurrent parameter – the effective impulse voltage U_D. However, the results of study of the dependence of the coating parameters on U_D showed poor accuracy for determining δ and R_a (the error level is 0.89 and 0.74, respectively). A known effective way to increase the reliability of the established dependences is to use the linear regression technique. According to the results of the regression equations calculation, one can see that the reliability of the approximation between the values of the calculated and experimental data was 0.90 for the coating thickness values and 0.81 – for the roughness.

The registration of the AE amplitude in the monitoring mode allowed increasing the reliability and accuracy of determining the values of coating parameters when using the regression analysis. The results of the study of the recorded AE signals within the MAO modes set in the work showed several cycles of the increase and subsequent decrease in the amplitude. The causes for the change in the amplitude can be explained by the mechanism of the ongoing process of the oxide coating formation and growth under the conditions specified by the oxidation modes. Multiple formation of bubbles at the *OA* stage, which is not yet associated with the formation of sparks and micro-arcs on the anode surface, leads to coherent combining of an acoustic noise from their collapse and, as a consequence, to an increase in the amplitude of the AE signals [20]. The P_1 parameter defined as the *AN* period eliminates

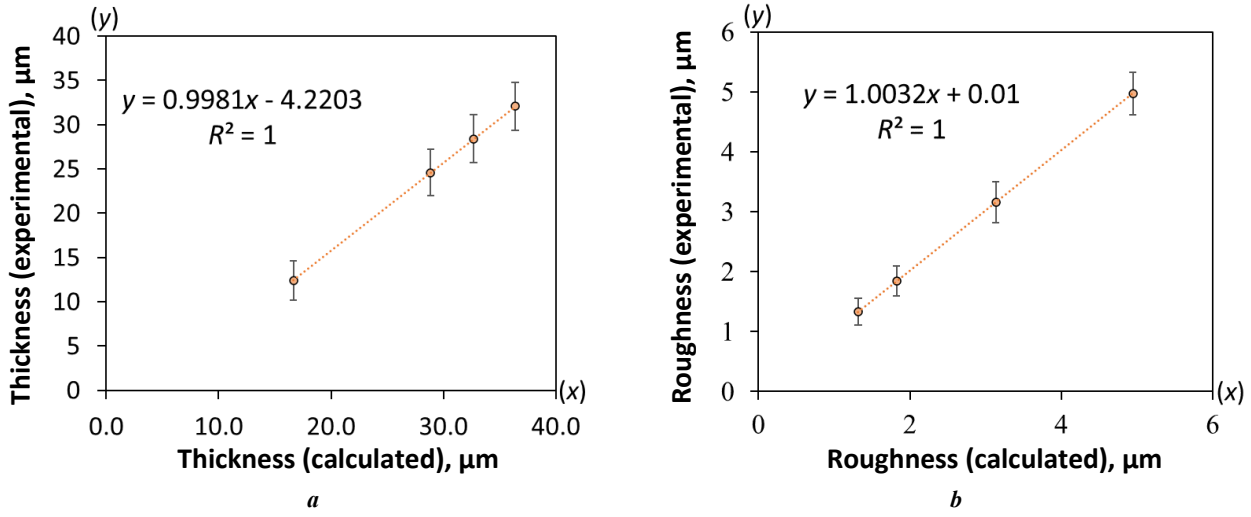

Fig. 10. *A graph relating the experimental and calculated values of the thickness δ* ***(a)*** *and roughness R_a* ***(b)*** *of the coating with the participation of the P_3 factor*
Рис. 10. *График, связывающий экспериментальные и расчетные значения толщины δ* ***(а)*** *и шероховатости R_a* ***(b)*** *покрытия при участии фактора P_3*

the negative effect of the initial *OA* period, when the electrical breakdowns have not yet begun, on the linear dependence determined by the regression equation. It explains the increase in the accuracy of determining the oxide coating thickness up to 0.93 and the roughness up to 0.82 when using the P_1 parameter as an additional factor.

The transition to the passivation state caused by the formation of a dense but still rather thin barrier layer leads to an increase in the size and a decrease in the number of bubbles occurring on the surface due to the formation of the first spark breakdowns, the number and energy of which gradually increase as the breakdown potential and the oxide film increase. Due to a change in the noise generation mechanism, the amplitude of the recorded AE signals first slightly decreases at the *AB* stage, but as the spark breakdown quantity and the oxide film thickness increase at the *BC* stage, it again increases. It is confirmed by the surface morphology of the coatings produced at various stages of oxidation. Fig. 3 a and 3 d show the coating surface obtained at the *AB* stage, where only multiple very-small-diameter channels are visible, characterizing the sparking onset. The replacement of the P_1 parameter in the regression analysis with the P_2 parameter determined by the *BN* period duration increases the accuracy of determining the coating thickness to 0.96 and the roughness – to 0.91.

Fig. 3 b and 3 e demonstrate the oxidized sample surface at the same current density at the end of the *BC* stage. One can assume that the *BC* stage is a transition stage between the spark and micro-arc oxidation processes. The increase in the amplitude of the AE signals is obviously associated with an increase in the pore diameter caused by an increase in the pulse energy as a result of sparking.

A further increase in the coating thickness at the *CN* stage first leads to a decrease in the number of breakdown channels, which are the centers of micro-arc discharges at this stage, and, as a result, to a certain decrease in the amplitude of the recorded AE signals. The use of the P_3 parameter determined by the *CN* period duration increased the accuracy of determining the thickness and roughness to 1. The results of the study demonstrate the importance of the influence of the oxidation duration at the final stage on the quality of the resulting coating.

The division of the oxidation time into periods characterizing a certain oxidation mechanism allows increasing the reliability of the relationship between the calculated and experimental values of the coating parameters.

It should be noted that the proposed approach has some constraints. These constraints include the absence of the P_2 and P_3 parameters for a certain ratio of oxidation time and current density, at which the oxidation process stays within the spark breakdown limits and does not go into the micro-arc mode. For these modes, either the *CN* stage or the *BC* and *CN* stages at the same time will be absent.

MAIN RESULTS AND CONCLUSIONS

The paper proposes a technique that allows establishing the dependence of the parameters of the oxide coating deposited on the D16AT aluminum alloy on various MAO modes. The technique is based on the solution of linear regression equations obtained as a result of an experiment with two factors: time and current density of oxidation. The reliability of the relationship between the experimental and calculated values of the oxide coating thickness and roughness was 0.89 and 0.74, respectively.

The introduction of an additional factor, defined as a period of time from the moment of reaching the minimum or maximum value of the AE signal amplitude cyclically changing during the oxidation process until the end of oxidation, increases the reliability of the linear approximation between the values of the coating parameters obtained experimentally or by calculation. The use of the time period from the moment of reaching the maximum value in the second cycle of the AE signal amplitude change to the oxidation process termination allows maximizing the reliability of the coating parameters' values obtained

by calculation as a result of solving the linear regression equations against the values obtained experimentally.

The addition of the proposed technique with a third controlled factor allows expanding its functionality and applying it in the online monitoring mode during the MAO process to increase the reliability of obtaining the specified values of the oxide coating thickness or roughness.

REFERENCES

1. Yerokhin A., Nie X., Leyland A., Matthews A., Dowey S. Plasma electrolysis for surface engineering. *Surface and coatings technology*, 1999, vol. 122, no. 2-3, pp. 73–93. DOI: 10.1016/S0257-8972(99)00441-7.
2. Pecherskaya E.A., Golubkov P.E., Karpanin O.V., Kozlov G.V., Zinchenko T.O., Smogunov V.V. The influence of technological parameters on the properties of coatings synthesized by microarc oxidation. *Izmerenie. Monitoring. Upravlenie. Kontrol*, 2020, no. 2, pp. 89–99. DOI: 10.21685/2307-5538-2020-2-11.
3. Shi M., Li H. The mathematical mode of Ti alloy micro-arc oxidation process parameters and ceramic coating and experimental study. *Journal of Yunnan University: Natural Sciences Edition*, 2015, vol. 37, no. 1, pp. 102–110.
4. Chen H., Hao J., Feng Z. Micro-arc oxidation mechanism and electrical discharge model. *Journal of Changan University (Natural Science Edition)*, 2008, vol. 28, pp. 116–119.
5. Golubkov P.E., Pecherskaya E.A., Artamonov D.V., Zinchenko T.O., Gerasimova Yu.E., Rozenberg N.V. Electrophysical model of micro-arc oxidation process. *Izvestiya vysshikh uchebnykh zavedeniy. Fizika*, 2019, vol. 62, no. 11, pp. 166–171. DOI: 10.17223/00213411/62/11/166.
6. Dudareva N.Yu., Akhmedzyanov D.A. Tribological parameters of MAO-layers formed in silicate-alkaline electrolyte on samples of high-silicon aluminum alloy AK12. *Vestnik Ufimskogo gosudarstvennogo aviatsionnogo tekhnicheskogo universiteta*, 2018, vol. 22, no. 3, pp. 10–16. EDN: YAAWLJ.
7. Pecherskaya E.A., Golubkov P.E., Melnikov O.A., Karpanin O.V., Zinchenko T.O., Artamonov D.V. Intelligent Technology of Oxide Layer Formation by Micro-Arc Oxidation. *IEEE Transactions on Plasma Science*, 2021, vol. 49, no. 9, pp. 2613–2617. DOI: 10.1109/TPS.2021.3091830.
8. Jayaraj R.K., Malarvizhi S., Balasubramanian V. Optimizing the micro-arc oxidation (MAO) parameters to attain coatings with minimum porosity and maximum hardness on the friction stir welded AA6061 aluminium alloy welds. *Defence technology*, 2017, vol. 13, no. 2, pp. 111–117. DOI: 10.1016/j.dt.2017.03.003.
9. Vakili-Azghandi M., Fattah-alhosseini A., Keshavarz M.K. Optimizing the electrolyte chemistry parameters of PEO coating on 6061 Al alloy by corrosion rate measurement: Response surface methodology. *Measurement*, 2018, vol. 124, pp. 252–259. DOI: 10.1016/j.measurement.2018.04.038.
10. Yang S. *On-line test method of micro-arc oxidation load impedance spectroscopy and on-line test system for realizing the method,* patent no. 102621391 CHN, 2012. 10 p.
11. Guo Y. *On-line Monitoring System of Micro-arc Oxidation Film Formation Process,* patent no. 111647924 CHN, 2021. 11 p.
12. Golubkov P.E. Analysis of the applicability of thickness measurement methods dielectric layers in controlled synthesis protective coatings by micro-arc method oxygenating. *Izmerenie. Monitoring. Upravlenie. Kontrol*, 2020, no. 1, pp. 81–92. DOI: 10.21685/2307-5538-2020-1-11.
13. Bespalova Zh.I., Panenko I.N., Dubovskov V.V., Kozachenko P.N., Kudryavtsev Yu.D. Investigation of the formation of optical black oxide-ceramic coatings on the surface of aluminum alloy 1160. *Izvestiya vysshikh uchebnykh zavedeniy. Severo-Kavkazskiy region. Estestvennye nauki*, 2012, no. 5, pp. 63–66. EDN: PFATGJ.
14. Mukaeva V.R., Gorbatkov M.V., Farrakhov R.G., Parfenov E.V. A study of the acoustic characteristics of plasma electrolytic oxidation of aluminum. *Elektrotekhnicheskie i informatsionnye kompleksy i sistemy*, 2018, vol. 14, no. 3, pp. 60–65. EDN: YSAZNZ.
15. Boinet M., Verdier S., Maximovitch S., Dalard F. Application of acoustic emission technique for in situ study of plasma anodizing. *NDT&E International*, 2004, vol. 37, no. 3, pp. 213–219. DOI: 10.1016/j.ndteint.2003.09.011.
16. Chen Z., Zhang L., Liu H. et al. 3D printing technique-improved phase-sensitive OTDR for breakdown discharge detection of gas-insulated switchgear. *Sensors*, 2020, vol. 20, no. 4, article number 1045. DOI: 10.3390/s20041045.
17. Bashkov O., Li X., Bao F., Kim V.A., Zhou C. Acoustic emission that occurs during the destruction of coatings applied by microarc oxidation on an aluminum alloy. *Materials Today: Proceedings*, 2019, vol. 19-5, pp. 2522–2525. DOI: 10.1016/j.matpr.2019.08.174.
18. Jadhav P., Bongale A., Kumar S. The effects of processing parameters on the formation of oxide layers in aluminium alloys using plasma electrolytic oxidation technique. *Journal of the Mechanical Behavior of Materials*, 2021, vol. 30, no. 1, pp. 118–129. DOI: 10.1515/jmbm-2021-0013.
19. Cao J., Fang Z., Chen J., Chen Z., Yin W., Yang Y., Zhang W. Preparation and Properties of Micro-arc Oxide Film with Single Dense Layer on Surface of 5083 Aluminum Alloy. *Journal of Chinese Society for Corrosion and Protection*, 2020, vol. 40, no. 3, pp. 251–258. DOI: 10.11902/1005.4537.2019.069.
20. Bashkov O.V., Bao F., Li X., Bashkova T.I. Investigation of the Influence of Electrical Modes on the Morphology and Properties of Oxide Coatings on Aluminum Alloy 1163, Obtained by the Micro-arc Oxidation. *Lecture notes in networks and systems*, 2021, vol. 200, pp. 87–95. DOI: 10.1007/978-3-030-69421-0_10.

СПИСОК ЛИТЕРАТУРЫ

1. Yerokhin A., Nie X., Leyland A., Matthews A., Dowey S. Plasma electrolysis for surface engineering // Surface and coatings technology. 1999. Vol. 122. № 2-3. P. 73–93. DOI: 10.1016/S0257-8972(99)00441-7.
2. Печерская Е.А., Голубков П.Е., Карпанин О.В., Козлов Г.В., Зинченко Т.О., Смогунов В.В. Влияние технологических параметров на свойства покрытий,

синтезируемых методом микродугового оксидирования // Измерение. Мониторинг. Управление. Контроль. 2020. № 2. С. 89–99. DOI: 10.21685/2307-5538-2020-2-11.
3. Shi M., Li H. The mathematical mode of Ti alloy micro-arc oxidation process parameters and ceramic coating and experimental study // Journal of Yunnan University: Natural Sciences Edition. 2015. Vol. 37. № 1. P. 102–110.
4. Chen H., Hao J., Feng Z. Micro-arc oxidation mechanism and electrical discharge model // Journal of Changan University (Natural Science Edition). 2008. Vol. 28. P. 116–119.
5. Голубков П.Е., Печерская Е.А., Артамонов Д.В., Зинченко Т.О., Герасимова Ю.Е., Розенберг Н.В. Электрофизическая модель процесса микродугового оксидирования // Известия высших учебных заведений. Физика. 2019. Т. 62. № 11. С. 166–171. DOI: 10.17223/00213411/62/11/166.
6. Дударева Н.Ю., Ахмедзянов Д.А. Трибологические параметры МДО-слоев, сформированных в силикатно-щелочном электролите на образцах из высококремниевого алюминиевого сплава АК12 // Вестник Уфимского государственного авиационного технического университета. 2018. Т. 22. № 3. С. 10–16. EDN: YAAWLJ.
7. Pecherskaya E.A., Golubkov P.E., Melnikov O.A., Karpanin O.V., Zinchenko T.O., Artamonov D.V. Intelligent Technology of Oxide Layer Formation by Micro-Arc Oxidation // IEEE Transactions on Plasma Science. 2021. Vol. 49. № 9. P. 2613–2617. DOI: 10.1109/TPS.2021.3091830.
8. Jayaraj R.K., Malarvizhi S., Balasubramanian V. Optimizing the micro-arc oxidation (MAO) parameters to attain coatings with minimum porosity and maximum hardness on the friction stir welded AA6061 aluminium alloy welds // Defence technology. 2017. Vol. 13. № 2. P. 111–117. DOI: 10.1016/j.dt.2017.03.003.
9. Vakili-Azghandi M., Fattah-alhosseini A., Keshavarz M.K. Optimizing the electrolyte chemistry parameters of PEO coating on 6061 Al alloy by corrosion rate measurement: Response surface methodology // Measurement. 2018. Vol. 124. P. 252–259. DOI: 10.1016/j.measurement.2018.04.038.
10. Yang S. On-line test method of micro-arc oxidation load impedance spectroscopy and on-line test system for realizing the method: patent № 102621391 CHN, 2012. 10 p.
11. Guo Y. On-line Monitoring System of Micro-arc Oxidation Film Formation Process: patent № 111647924 CHN, 2021. 11 p.
12. Голубков П.Е. Анализ применимости методов измерения толщины диэлектрических слоев при управляемом синтезе защитных покрытий методом микродугового оксидирования // Измерение. Мониторинг. Управление. Контроль. 2020. № 1. С. 81–92. DOI: 10.21685/2307-5538-2020-1-11.
13. Беспалова Ж.И., Паненко И.Н., Дубовсков В.В., Козаченко П.Н., Кудрявцев Ю.Д. Исследование процесса формирования оптически черных оксидно-керамических покрытий на поверхности алюминиевого сплава 1160 // Известия высших учебных заведений. Северо-Кавказский регион. Естественные науки. 2012. № 5. С. 63–66. EDN: PFATGJ.
14. Мукаева В.Р., Горбатков М.В., Фаррахов Р.Г., Парфенов Е.В. Исследование акустических характеристик процесса плазменно-электролитического оксидирования алюминия // Электротехнические и информационные комплексы и системы. 2018. Т. 14. № 3. С. 60–65. EDN: YSAZNZ.
15. Boinet M., Verdier S., Maximovitch S., Dalard F. Application of acoustic emission technique for in situ study of plasma anodizing // NDT&E International. 2004. Vol. 37. № 3. P. 213–219. DOI: 10.1016/j.ndteint.2003.09.011.
16. Chen Z., Zhang L., Liu H. et al. 3D printing technique-improved phase-sensitive OTDR for breakdown discharge detection of gas-insulated switchgear // Sensors. 2020. Vol. 20. № 4. Article number 1045. DOI: 10.3390/s20041045.
17. Bashkov O., Li X., Bao F., Kim V.A., Zhou C. Acoustic emission that occurs during the destruction of coatings applied by microarc oxidation on an aluminum alloy // Materials Today: Proceedings. 2019. Vol. 19-5. P. 2522–2525. DOI: 10.1016/j.matpr.2019.08.174.
18. Jadhav P., Bongale A., Kumar S. The effects of processing parameters on the formation of oxide layers in aluminium alloys using plasma electrolytic oxidation technique // Journal of the Mechanical Behavior of Materials. 2021. Vol. 30. № 1. P. 118–129. DOI: 10.1515/jmbm-2021-0013.
19. Cao J., Fang Z., Chen J., Chen Z., Yin W., Yang Y., Zhang W. Preparation and Properties of Micro-arc Oxide Film with Single Dense Layer on Surface of 5083 Aluminum Alloy // Journal of Chinese Society for Corrosion and Protection. 2020. Vol. 40. № 3. P. 251–258. DOI: 10.11902/1005.4537.2019.069.
20. Bashkov O.V., Bao F., Li X., Bashkova T.I. Investigation of the Influence of Electrical Modes on the Morphology and Properties of Oxide Coatings on Aluminum Alloy 1163, Obtained by the Micro-arc Oxidation // Lecture notes in networks and systems. 2021. Vol. 200. P. 87–95. DOI: 10.1007/978-3-030-69421-0_10.

Исследование влияния режимов микродугового оксидирования на морфологию и параметры оксидного покрытия, наносимого на алюминиевый сплав Д16АТ

Бао Фэнюань[1,3], младший научный сотрудник, инженер-исследователь
Башков Олег Викторович*[1,4], доктор технических наук, профессор,
заведующий кафедрой «Материаловедение и технология новых материалов»
Чжан Дан[2,5], доктор технических наук, профессор, заведующий лабораторией «Машиностроение»
Люй Лань[1,2], аспирант
Башкова Татьяна Игоревна[1,6], кандидат технических наук, доцент
[1]*Комсомольский-на-Амуре государственный университет, Комсомольск-на-Амуре (Россия)*
[2]*Хэйлунцзянский университет науки и технологий, Харбин (Китай)*

***E-mail: bashkov@knastu.ru**

[3]ORCID: https://orcid.org/0000-0001-5762-7953
[4]ORCID: https://orcid.org/0000-0002-3910-9797
[5]ORCID: https://orcid.org/0000-0003-4150-7038
[6]ORCID: https://orcid.org/0000-0001-7070-5821

Поступила в редакцию 06.12.2022 *Принята к публикации 19.01.2023*

Аннотация: Эффективным способом защиты вентильных металлов и их сплавов является метод микродугового оксидирования (МДО), в настоящее время применяемый в различных отраслях. Однако для достижения желаемых характеристик и свойств оксидных покрытий требуется большое число экспериментов по определению оптимального режима оксидирования, что делает метод МДО трудоемким и ресурсозатратным. Одним из путей решения данной проблемы является поиск информативного параметра или нескольких параметров, использование которых при мониторинге процесса оксидирования позволит установить связь между режимами МДО и заданными характеристиками оксидных покрытий. В работе изучено влияние заданных технологических режимов МДО (плотности тока, времени оксидирования, регистрируемой в процессе МДО амплитуды сигналов акустической эмиссии (АЭ)) на морфологию и параметры оксидных покрытий (толщину δ и шероховатость поверхности R_a), наносимых на алюминиевый сплав Д16АТ, плакированный чистым алюминием. Многофакторное планирование эксперимента и проведенный регрессионный анализ позволили установить связь между двумя факторами оксидирования (плотностью тока и временем оксидирования) и параметрами получаемых покрытий. Предложен дополнительный фактор, определяемый в режиме мониторинга в процессе оксидирования как время от момента достижения максимума или минимума регистрируемой в процессе МДО амплитуды АЭ до окончания процесса оксидирования. Установлено, что введение дополнительного фактора позволяет существенно повысить достоверность зависимости между параметрами покрытий, получаемыми экспериментально и расчетным методом на основе регрессионного анализа. Отмечено, что при выполнении МДО высокая достоверность между расчетными и фактическими значениями параметров оксидных покрытий может быть достигнута при дополнительном мониторинге процесса МДО путем регистрации амплитуды АЭ.

Ключевые слова: микродуговое оксидирование; оксидное покрытие; акустическая эмиссия; многофакторный анализ; морфология поверхности; алюминиевый сплав; Д16АТ; сплавы вентильной группы.

Благодарности: Работа выполнена при поддержке гранта Президента РФ для государственной поддержки ведущих научных школ Российской Федерации (проект НШ-452.2022.4).

Для цитирования: Бао Ф., Башков О.В., Чжан Д., Люй Л., Башкова Т.И. Исследование влияния режимов микродугового оксидирования на морфологию и параметры оксидного покрытия, наносимого на алюминиевый сплав Д16АТ // Frontier Materials & Technologies. 2023. № 1. С. 7–21. DOI: 10.18323/2782-4039-2023-1-7-21.